

Reduced saturation magnetization in cobalt antidot thin films prepared by polyethylene oxide-assisted self-assembly of polystyrene nanospheres

Chi-Chih Ho,¹ Tung-Wu Hsieh,¹ Hsiang-Hsi Kung,¹ Wen-Tau Juan,¹ Keng-Hui Lin,^{1,2} and Wei-Li Lee^{1,a)}

¹*Institute of Physics, Academia Sinica, Nankang, Taipei 11529, Taiwan*

²*Research Center of Applied Science, Academia Sinica, Nankang, Taipei 11529, Taiwan*

(Received 12 January 2010; accepted 2 March 2010; published online 23 March 2010)

We have developed an approach to prepare large array nanostructured thin films using polyethylene oxide assisted self-assembly of polystyrene nanospheres as a template. By tuning the antidot diameter in the cobalt thin films, we found a crossover behavior in the magnetization reversal process. In addition, the effective moment per cobalt atom turns out to drop with growing antidot diameter which effectively increases the surface to bulk volume fraction. Our results suggest a tendency of reduced saturation magnetization in a ferromagnet/normal metal interface, where the mixing of itinerant electrons with ferromagnetic d electrons can give rise to observable effect. © 2010 American Institute of Physics. [doi:10.1063/1.3371692]

Nanotechnology has long been a major research interest that promises grand challenge and large impact to current science and technology. The quest for large array nanostructure emerges in many fields, including magnetic storage industry, photonic crystal, artificial surface roughening, etc. In magnetic storage industry, the development in the hard disk drive (HDD) areal density is quite impressive starting from few kbits/in² in 1950s to 170 Gbits/in² in the latest HDD nowadays. As the single bit scales down in size, the surface to bulk volume fraction in a ferromagnet scales up. Therefore, it would be important to understand the magnetic property in the surface layer of a ferromagnet. Previous works in ferromagnetic ultrathin film and nanocluster prepared and characterized in ultrahigh vacuum suggest an increase in saturation magnetization.^{1,2} However, much less is known in the case of magnetism at the interface between a ferromagnet and a nonmagnetic material, which is normally the case in practical device.

In 1995, Hulthen and van Duyne pioneered the nanosphere (NS) lithography (Refs. 3 and 4) to fabricate large area nanostructures by employing commercially available monodisperse polystyrene nanospheres, from 10 nm to several micrometers in diameter. Under appropriate conditions such as spin coating⁵ and vertical pulling,⁶ the NSs assemble into crystalline structure and serve as a mask for thin film deposition or pattern etching. Many techniques rely on the interfacial properties which are substrate dependent. The NSs packing domains are usually of order of a few square micrometers due to the instability during the solvent evaporation. Having an intermediate step to assemble NSs in water/air interface and then transfer onto a substrate turns out a feasible method. By further adding trace amount of polyethylene oxide (PEO) long chain polymers with molecular weight $M_w = 145\,000\,0\text{ g mol}^{-1}$ in the water, the adsorption of PEO onto the PS NSs (Ref. 7) results in the polymer bridging effect which makes the NSs at the water surface to connect through PEO and form robust NSs membrane against the surface tension tearing during the NSs transfer process. Further discussion on the mechanism of PEO-

assisted self-assembly will be described in a separate paper. Figures 1(a) and 1(b) show the images of monolayer NSs with diameter 1 μm and 220 nm, respectively, on a silicon(100) substrate prepared by this approach. The defect-free region is more than $100 \times 100\ \mu\text{m}^2$ for 1 μm NSs and $20 \times 20\ \mu\text{m}^2$ for 220 nm NSs, which roughly scales with the NSs size. We remark that the entire substrate area up to $1 \times 1\ \text{cm}^2$ are uniformly covered by the monolayer NSs. Even though it may not be single packing domain, the NSs are in contact with each other and have no major cracks or vacancies. This allows us to achieve the highest number density and perform quantitative analysis.

We prepared a large area monolayer of close-packed PS NSs with diameter 220 nm onto a silicon(100) substrate using the procedure described previously. Utilizing the oxygen ion etching, the diameter of NSs can be tuned as much as by half without serious influence on their shape and position. A cobalt thin film was then deposited from a cobalt target with 99.99% purity using a magnetron sputtering system followed by a 3 nm platinum (Pt) deposition as the capping layer to prevent oxidation in the cobalt thin film. The chamber base pressure and sputtering pressure are 4×10^{-9} Torr and 6 m Torr, respectively. At last, large area cobalt antidot thin films were obtained after removing the NSs. In order to avoid the oxidation on the side wall of the cobalt thin film, we further used an argon ion mill system to clean the surface followed again by 3 nm Pt as a capping layer. We have prepared two series of cobalt antidot samples with cobalt film thickness

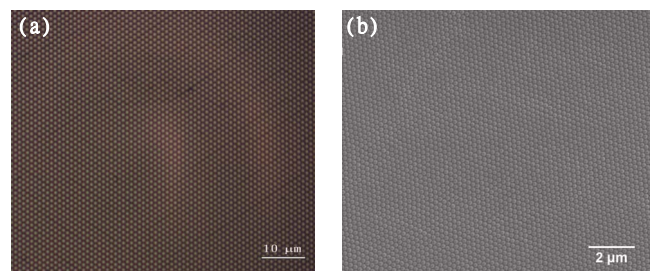


FIG. 1. (Color online) (a) Optical microscope image of a monolayer 1 μm NSs on Si(100) substrate. (b) SEM image of a monolayer 220 nm NSs on Si(100) substrate.

^{a)}Electronic mail: wlee@phys.sinica.edu.tw.

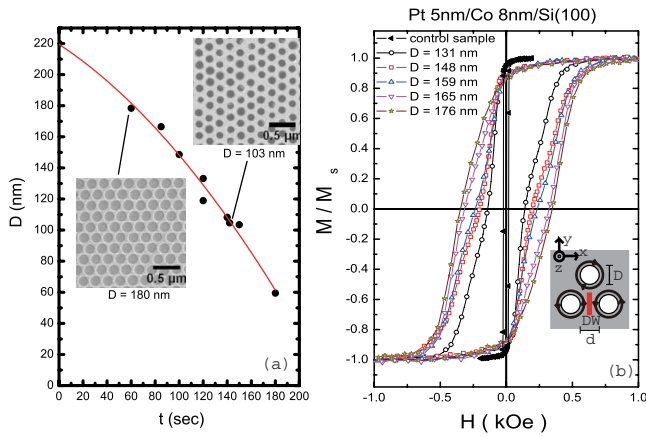


FIG. 2. (Color online) (a) NSs diameter D as a function of oxygen ion etching time. The upper and lower inset shows the SEM images of cobalt antidot thin films with antidot diameter D equals 103 and 180 nm, respectively. (b) Normalized magnetization vs in-plane field H for a series of Pt(5 nm)/Co(8 nm)/Si(100) antidot thin films with five different values of antidot diameter D and one control sample. The inset illustrates the vortex state configuration for $D < 160$ nm.

t equals 8 and 19 nm. Each series contains five samples with different sizes of antidot and one control sample that has no antidot. The antidot diameter D is determined by averaging over 20 SEM images containing more than 25 000 antidots in total.¹³ Fig. 2(a) plots the oxygen ion etching time t as a function of the resulting antidot diameter D . The data points can fit well to the relation of $D = \sqrt{D_0^2 - \alpha t}$ shown as red line in the figure, where D_0 equals 220 nm and α is a constant depending on the etching condition.

Magnetic property of the cobalt antidot thin films were detected by a vibrating sample magnetometer (VSM). Figure 2(b) shows the in-plane magnetic field dependence of the magnetization in Pt 3 nm/Co 8 nm/Si(100) antidot thin films with five different values of antidot diameter D ranging from 131 to 176 nm and one control sample. The magnetization reversal for all the antidot samples exhibits much broader width compared to the control sample. For $D < 160$ nm, upon reversing the magnetic field, the magnetization initially drops rapidly to nearly zero followed by a slower increase in magnetization. This feature resembles the behavior in a magnetic nanoring system that may suggest the formation of vortex state in low field.⁸ The possible magnetic configuration of the vortex state is illustrated in the inset of Fig. 2(b) where the black line with arrows represents magnetization orientation and the thick red line indicates a domain wall. On the other hand, for $D > 160$ nm, the hysteresis loops restore the behavior of typical magnetization reversal through domain walls. From the angular remanence measurements, the control sample shows clear uniaxial magnetic anisotropy and larger remanence along easy axis which is typical for a sputtered magnetic thin film. On the contrary, the hysteresis loops shown in Fig. 2(b) do not vary significantly with the magnetic field orientation.

The magnetic moment approaches a constant value when the field goes above 500 Oe as shown in Fig. 2(b). Further increment of the field up to 10 000 Oe only reduces the magnetic moment because of the diamagnetic contribution from the substrate. We then determined the saturation magnetization M_s in units of Bohr magneton μ_B per cobalt atom in our antidot samples using the antidot diameter D obtained from statistic averaging over 20 SEM images as mentioned earlier.

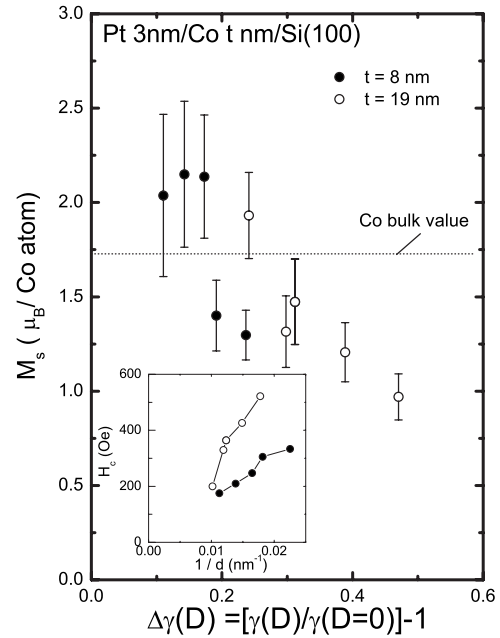


FIG. 3. Saturation magnetization M_s vs surface to bulk volume fraction increase $\Delta\gamma$ in two series of cobalt antidot thin films. Solid circles and open circles represent samples with cobalt film thickness $t=8$ nm and 19 nm, respectively. Lower inset shows the corresponding magnetic coercivity H_c vs $1/d$, where d is the mean separation between antidots. The dotted line is the M_s value of a bulk cobalt.

Figure 3 plots the M_s versus surface to bulk volume fraction increase $\Delta\gamma$, where $\Delta\gamma = [\gamma(D)/\gamma(D=0)] - 1$. $\gamma(D=0)$ is the surface to bulk volume fraction of a control sample without antidots. The surface regions locate at the upper and lower parts of a cobalt thin film corresponding to Pt/Co interface and Co/SiO₂ interface, respectively. Upon introducing antidots into the cobalt thin films, both the cobalt surface and bulk volume reduced while there is a compensation in the surface volume coming from the antidots' side-wall Pt/Co interface. The bigger the D is, the larger the $\gamma(D)$ would be. Even though the exact value of $\gamma(D=0)$ is unknown, the percentage increase in the surface to bulk volume fraction $\Delta\gamma$, with respect to the control sample, can be well determined. The error bar indicates the standard deviation of antidot diameter D arising from statistic averaging. We found that the M_s tends to decrease at larger $\Delta\gamma$ within the error. For cobalt antidot films with $t=19$ nm, $\Delta\gamma$ reaches 50% for $D=163$ nm. The corresponding M_s drops to a value of 1.0 μ_B per cobalt atom. For thinner cobalt antidot films with $t=8$ nm, the gain in surface to bulk volume fraction is smaller giving a $M_s=1.3$ μ_B per cobalt atom for $D=176$ nm. The figure shows a clear trend that M_s is marching down with increasing surface to bulk volume fraction. The inset of Fig. 3 indicates the monotonic increase in coercive field H_c with $1/d$, where $d \equiv 220 - D$ (nm) is the mean separation between antidots.

For small antidot diameter D , the minimum energy criteria favors the occurrence of vortex state in regions around antidots where domain walls inevitably occur between vortices. As D increases, the mean separation d between antidots eventually reduces to a value smaller than the expected domain wall width. In this case, the vortex state is no longer a stable magnetic configuration and does not appear in the magnetization reversal process at large D giving rise to the crossover behavior in the hysteresis loops shown in Fig. 2(a).

From the hysteresis loops along easy and hard axis, we determined the uniaxial anisotropy constant $K_u \approx 5 \times 10^4$ erg/cm³ in the control sample with $t=8$ nm. In the thin film limit ($t \ll \delta_{DW}$), the Néel type domain wall is energetically favorable with the corresponding domain wall width $\delta_{DW} \approx \pi\sqrt{2A/K_u}$, where $A \approx 1 \times 10^{-6}$ erg/cm is the exchange stiffness for cobalt. The domain wall width δ_{DW} is calculated to be about 200 nm. Although we failed to extract the K_u in antidot samples because of the multiple packing domains, we argue that the K_u is enhanced at larger D due to the implement of shape anisotropy resulting in a smaller δ_{DW} than 200 nm. This could then make the δ_{DW} falling in the range of d in our experiment ($40 \text{ nm} \leq d \leq 90 \text{ nm}$), which is in accord with the scenario we proposed earlier for the crossover behavior. On the other hand, we note that for cobalt antidot thin films with $t=19$ nm (not shown), no crossover to vortex state was observed. We suspect that the δ_{DW} becomes larger compared to $t=8$ nm samples due to smaller K_u . This is true for the control sample with $t=19$ nm where its K_u is threefolds smaller. Therefore, the vortex state becomes unfavorable according to the scenario. However, the micromagnetic simulations using OOMMF package were unable to reproduce the hysteresis loops observed in our experiment. In addition, previous works in iron and Permalloy antidot array¹⁰ did not report similar crossover behavior in magnetization reversal when tuning the antidot diameter. Further investigation is required to identify its true mechanism.

We now turn to the issue concerning the reduced saturation magnetization M_s in our cobalt antidot thin films. We performed the hysteresis loop measurement at 5 K after field cooling from 400 K at 2000 Oe. No exchange bias effect⁹ from antiferromagnetic cobalt oxide ($T_N \approx 290$ K) (Ref. 11) was ever observed in our samples.¹³ The reduction in the M_s due to oxidation effect can then be excluded. In addition, we also performed vector VSM measurement on antidot samples. At large in-plane field applied along x axis, the M_y and M_z components are less than 1% of M_x . We, therefore, conclude that the reduced M_s is an intrinsic property in the thin film. According to theoretical calculation,¹² the M_s for the surface layer of a ferromagnet is enhanced owing to the reduced coordination number and reduced bonding which make the surface d states more localized. On the other hand, the calculation also suggests that at the interface region between a ferromagnetic film and a conducting substrate, such as copper, the M_s is reduced instead. The reduction of the M_s at the interface region is a consequence of mixing the itinerant electrons in the substrate with the ferromagnetic d electrons. Therefore, the reduced M_s in our cobalt antidot thin films is more likely associated with the mixing effect at the Pt/Co interface. In principle, different capping material may give rise to different level of mixing.

In conclusion, we developed a scheme to prepare monolayer of NSs onto a substrate of any kind. The NSs at the water/air interface are closely packed and linked together through the PEO bridging effect. They constitute a robust membrane of hexagonal-packed structure that can be transferred to a substrate without breaking. From the magnetization measurements of the Pt/Co/Si(100) antidot thin films with cobalt thickness of 8 and 19 nm, we observed a crossover behavior in magnetization reversal process as antidot diameter D decreases in thinner film that possesses higher magnetic anisotropy. We also found that the effective moment per cobalt atom tends to drop lower than the bulk value as the surface to bulk volume fraction increases. We attribute this phenomena to be the mixing of itinerant electrons with ferromagnetic d electrons at the Pt/Co interface. However, the issue concerning the depth of mixing and also the role of the capping material remains an open question and requires further investigation. This would be crucial in designing ultrahigh density data storage device based on nanostructured magnetic thin film.

The authors acknowledge the funding support from National Science Council in Taiwan and Nanoscience Program at Academia Sinica, Taipei.

- ¹F. Huang, M. T. Kief, G. J. Mankey, and R. F. Willis, *Phys. Rev. B* **49**, 3962 (1994).
- ²J. P. Bucher, D. C. Douglass, and L. A. Bloomfield, *Phys. Rev. Lett.* **66**, 3052 (1991); J. Merikoski, J. Timonen, M. Manninen, and P. Jena, *ibid.* **66**, 938 (1991).
- ³Y. Xia, B. Gates, Y. Yin, and Y. Lu, *Adv. Mater. (Weinheim, Ger.)* **12**, 693 (2000).
- ⁴J. C. Hulthén and R. P. Van Duyne, *J. Vac. Sci. Technol. A* **13**, 1553 (1995).
- ⁵C.-W. Kuo, J. Y. Shiu, Y. H. Cho, and P. Chen, *Adv. Mater.* **15**, 1065 (2003).
- ⁶A. S. Dimitrov and K. Nagayama, *Langmuir* **12**, 1303 (1996); S. M. Weekes, F. Y. Ogrin, W. A. Murray, and P. S. Keatley, *ibid.* **23**, 1057 (2007); F. Pan, J. Zhang, C. Cai, and T. Wang, *ibid.* **22**, 7101 (2006).
- ⁷D. Qiu, T. Cosgrove, P. Revell, and I. Howell, *Macromolecules* **42**, 547 (2009).
- ⁸M. Kläui, J. Rothman, L. Lopez-Diaz, C. A. F. Vaz, and J. A. C. Bland, *Appl. Phys. Lett.* **78**, 3268 (2001); F. Q. Zhu, G. W. Chern, O. Tchernyshyov, X. C. Zhu, J. G. Zhu, and C. L. Chien, *Phys. Rev. Lett.* **96**, 027205 (2006).
- ⁹L. I. Balcells, B. Martinez, O. Iglesias, J. M. Garcia-Martin, A. Cebollada, A. Garcia-Martin, G. Armelles, B. Sepulveda, and Y. Alaverdyan, *Appl. Phys. Lett.* **94**, 062502 (2009); D. Buntinx, S. Brems, A. Volodin, K. Temst, and C. Van Haesendonck, *Phys. Rev. Lett.* **94**, 017204 (2005).
- ¹⁰I. Guedes, M. Grimsditch, V. Metlushko, P. Vavassori, R. Camley, B. Ilic, P. Neuzil, and R. Kumar, *Phys. Rev. B* **66**, 014434 (2002); P. Vavassori, G. Gubbiotti, G. Zangari, C. T. Yu, H. Yin, H. Jiang, and G. j. Mankey, *J. Appl. Phys.* **91**, 7992 (2002); C. C. Wang, A. O. Adeyeye, and N. Singh, *Nanotechnology* **17**, 1629 (2006).
- ¹¹J. Nogués and I. K. Schuller, *J. Magn. Magn. Mater.* **192**, 203 (1999).
- ¹²J. Tersoff and L. M. Falicov, *Phys. Rev. B* **26**, 6186 (1982); for a review, see R. C. O. Handley, *Modern Magnetic Materials* (John Wiley and Sons, Hoboken, 1999), Chap. 16.
- ¹³See supplementary material at <http://dx.doi.org/10.1063/1.3371692> for SEM image analysis and vector VSM results.